This article has been published in Bone. The final publication is available at Elsevier via https://doi.org/10.1016/j.bone.2020.115304

A search for apatite crystals in the gap zone of collagen fibrils in bone using dark-field illumination

Schwarcz H.P[1,2]., Binkley D.M.[3], Luo L.[4], and Grandfield K[2,3]

[1]School of Geography and Earth Science

[2]School of Biomedical Engineering, McMaster University, Hamilton, Ontario, Canada

[3]Department of Materials Science and Engineering, McMaster University, Hamilton, Ontario, Canada

[4]Faculty of Health Sciences, McMaster University, Hamilton, Ontario, Canada

Abstract

Bright-field transmission electron microscope (TEM) images of ion milled or focused ion beam (FIB) sections of cortical bone sectioned parallel to the long axis of collagen fibrils display an electron-dense phase in the gap zones of the fibrils, as well as elongated plates (termed mineral lamellae) comprised of apatite crystals, which surround and lie between the fibrils. Energy dispersive X-ray spectroscopy (EDS) and electron energy loss spectroscopy (EELS) studies by others have shown that the material in the gap zones is calcium phosphate. Dark-field (DF) images are capable of revealing the projected position of crystals of apatite in a section of bone. We obtained bright field (BF) images of ion milled sections of bovine femoral cortical bone cut parallel to fibril axes (longitudinal view), and compared them with DF images obtained using the (002) apatite reflection to test a widely held theory that most of the mineral in bone resides in the gap zones. Most apatite crystals which were illuminated in DF images and which projected onto gap zones were extensions of crystals that also project onto adjacent overlap zones. However, in BF images, overlap zones do not appear to contain significant amounts of mineral, implying that the crystals imaged in DF are actually in the interfibrillar matrix but projected onto images of fibrils. However a small number of "free" illuminated crystals did not extend into the overlap zones; these could be physically located inside the gap zones. We note that projections of gap zones cover 60% of the area of any longitudinal field of view; thus these "free" crystals have a high random probability of appearing to lie on a gap zone, wherever they physically lie in the

section. The evidence of this study does not support the notion that most of the mineral bone consists of crystals in the gap zone. This study leaves uncertain what is the Ca-P containing material present in gap zones; a possible candidate material is amorphous calcium phosphate.

Key words: TEM, bright field, dark field, bone ultrastructure, fibril, gap zone, apatite crystals, mineral lamellae

1. Introduction

Bone is widely recognized to be a composite material made up principally of two components: collagen and mineral. Triple helices of Type I collagen are assembled into fibrils which are closely associated with plate-like crystals of apatite. The c-axes of the apatite are aligned approximately parallel to the long axes of the collagen fibrils [1]. Using sections prepared by either ion milling or focused ion beam (FIB) methods, we have shown in previous work that the majority of the mineral in bone occurs outside the collagen fibrils in the form of elongated plates, 100s of nm long, approximately 5 nm thick, and 60 to 80 nm wide [1, 2]. Using dark field (DF) imaging, it was possible to show that the plates are mosaics of single crystals, 5 nm thick and a few tens of nm across [3], approximately the same dimensions as single crystals that had been previously obtained by removing collagen from samples of powdered bone by chemical oxidation [4]. These plates range from being curved and wrapped around the fibrils, to flat plates which lie between adjacent fibrils. They have been referred to as *mineral lamellae* (MLs) [5]. This term refers specifically to the polycrystalline, 5-6 nm thick plates which we have observed in all bone samples studied by us. We use this term in preference to less specific terms such as “platelet” and “mineral particle” which have been used elsewhere in the literature. McNally *et al*. [1] showed that most of the mineral in bone (~ 80%) is in the form of these extrafibrillar plates.

However, it has long been apparent that some mineral also occurs within the collagen fibrils. In bright-field (BF) images of sections of bone prepared either by ion milling or by microtome sectioning, periodic electron-dense bands 40 nm wide are seen oriented perpendicular to the long axes of the fibrils, and spaced about 67 nm apart (Fig 1). These have been interpreted as showing the presence of mineral in the so-called gap zones along which occur 40 nm-long gaps between the ends of collinear collagen molecules [6–8]. Adjacent to each gap zone is an “overlap zone” in which no excess electron density is observed. Using either electron energy loss spectroscopy

(EELS) or energy-dispersive X-ray spectroscopy (EDS) it has been found that the gap zones contain substantial concentrations of Ca and P [9–11], supporting the notion that they contain crystals of a Ca phosphate mineral.

For each BF TEM image of bone, we can obtain a selected-area electron diffraction pattern (SAED) showing rings which correspond to the positions of Bragg-reflections from crystal lattice planes (Fig 2). The rings can be indexed to the lattice planes of apatite (all apatites including hydroxyapatite give essentially the same diffraction pattern). If we place an aperture on part of one of these rings and create an image using only the electrons scattered through that aperture, then we obtain an image of only those crystals which were appropriately oriented so that they could diffract electrons [12]. These are called dark-field (DF) images. They allow us to test two kinds questions: a) what are the shapes and sizes of single crystals of apatite in bone?; and b) what is the spatial relationship of the apatite crystals to each other and to features previously visualized in BF images of the same field of view?

Since gap zones contain significant amounts of Ca and P, we could use the DF method to test whether crystals of apatite are located in them. In essence, this was the goal of the present paper.

1.1 Three-dimensional form of bone and nature of TEM images

BF images of sections of bone such as Fig 1 represent projections of the three-dimensional (3D) form of an approximately 100 nm-thick sections of bone onto the projection plane. As a result there is some uncertainty in interpreting the relation between mineral and collagen from the 2D images. Fortunately, as a result of our previous studies of images of orthogonal sections bone, it is possible to reconstruct some general features of the 3D form of the section and recognize the effects of superposition of objects within this section. Fig 3 shows a schematic view of a 100 nm-thick block of bone cut so that it can be viewed in the TEM through a plane oriented parallel to the collagen fibrils (the X-Y plane in Fig 1). Sections cutting transversely through the fibrils are seen in the X-Z planes; mainly these appear to be empty holes or partially filled with low-contrast material. We have shown that in bone these holes are filled with collagen but that in TEM sections the collagen is partially or wholly eroded away by the ion beam [13]. From Fig 3 we see that any electron path directed normal to and passing through the X-Y plane will pass through one or two 50 nm-diameter fibrils within the sample. Gap zones extend continuously

across the X-Y plane, defined by zones of higher electron density. However, from Fig 3 we see that this continuity of gap zones is a result of two facts: a) the fibrils are vertically superimposed in a staggered array; and b) the gap zones in adjacent fibrils are always in register.

The gap zones provide a convenient means for identifying the presence of a collagen fibril at some depth (Z coordinate) in the section beneath a given point on the X-Y plane. However, note that the gap zones extend *continuously* across the width of the fields of view of all longitudinal sections of bone. This tells us that collagen fibrils are universally present at some depth under any point in the X-Y plane.

As a result of the superposition of fibrils, it is in general difficult to know whether a particular feature (e.g. an apatite crystal) seen in a BF or DF image is inside a fibril or in the surrounding mineralized matrix. However, we have just shown that *every* object seen on the X-Y plane must be projected onto a collagen fibril whether or not the object physically resides inside the fibril. Recollecting that gap zones occupy 60% of the volume of fibrils [14], there is a 0.6 probability that any object seen projected onto a fibril will overlap the image of a gap zone, whether or not the object is physically located inside the gap zone.

1.2 Plan of the study

The goal of the present study is to test the widely held hypothesis that most or at least many of the apatite crystals found in bone are physically located inside the fibrils, and more specifically within the gap zones. The approach to this is as follows. First we demonstrate typical BF images of longitudinal sections of bone, to show the apparent location and form of some of the crystalline plates (mineral lamellae) that surround collagen fibrils, as well as the partial electron opacity associated with the 40 nm-wide gap zones. We then present DF images of the same field of view, using the (002) reflections. We have also superimposed the positions of the gap zones (taken from the BF image) on the DF image. Following this, we report on the occurrence of DF images of apatite crystals that appear to be only confined to gap zones, rather than DF images of crystals which are clearly parts of MLs that extend beyond the boundaries of the gap zone in question. Presence of images of the former type would partially confirm the existence and allow us to estimate the abundance of crystals physically within the gap zones. We also show one

example of the corresponding BF/DF images obtained using a number of other Bragg reflections to test whether they add information to this inquiry.

2. Methods

A section of the cortex of the femoral diaphysis of a mature cow (*Bos taurus*) was prepared for electron microscopy by ion milling (see Supplementary Material). The sample had been frozen soon after euthanasia. After thawing of a small piece of this bone, and prior to sectioning, the sample was fixed in formalin, then dehydrated and stored in 100% ethanol. Previous studies have shown that this mode of fixing has no effect on the ultrastructural relations of the mineral and associated collagen [10]. The section was cut parallel to the long axis of the femur so that the collagen fibrils would tend to lie in the plane of the section. The section was viewed in both BF and DF using a Phillips CM12 TEM operated at 120 kV.

DF images were obtained by placement of a 100 nm diameter aperture on the (002) reflections of apatite in the SAED pattern obtained from each BF image. The (002) reflections form two partial arcs with an angular spread of about 30^{0} in each, centered on the azimuth of the fibril axis (Fig. 2). This is because the c-axes of apatite crystals in bone are oriented approximately parallel to the axes of collagen fibrils and also approximately parallel to the long axis of the long bone from which the sample was taken [10, 15]. As noted earlier, most of the apatite in bone is in the form of plates which can be viewed edgewise in sections cut parallel to the fibril axes; only those plates which are oriented with their flat surfaces oriented normal to the plane of the section ("edgewise") can be seen, while the remainder, at angles closer to the plane of the section, cannot be resolved, although their presence can be inferred from their appearance in sections cut normal to the fibrils (X-Z face in Fig. 3). Their invisibility in the BF images is due to their comparative thinness in this orientation resulting in less scattering of electrons. For the same reason, only crystals oriented edgewise to the plane of the section are visible in DF images. As a result, DF illuminated features are mostly rectangular areas 5 nm thick and a few tens of nm long corresponding to the size and shape of sections of crystals in MLs [16].

The preferential orientation of the mineral lamellae accounts for part of the concentration of c-axes parallel to the fibril as seen in the SAED pattern. However, any other apatite crystals in the sample (e.g., in the gap zones) must also share this orientation if they are large enough to

Bragg scatter electrons, since the arcs of the SAED pattern (Fig 2) shows that the c-axes of all apatite crystals in bone are oriented approximately parallel to the collagen fibrils. Some crystals in the section are not correctly oriented to scatter electrons into the DF image, even though they are in the form of plates aligned with the fibrils, because the c-axis of the crystals is tilted too far away from the plane of the section. Therefore we will unavoidably miss seeing the locations of some crystals in the DF image. However, we assume that this loss is random and that a representative population of crystals from any given structure would still be visible. The same would be true of crystals in the gap zones.

The aperture used for the DF image allows us to capture electrons from only a small angular range of the total arc of (002) reflections. This in turn allows us to visualize in DF only crystals with a specific azimuthal orientation (Fig 4). This figure shows that by moving the aperture along the (002) arc, we are able to capture the DF images of crystals whose c-axes vary in orientation. In order to capture the images of a larger range of crystals in each field of view, we prepared successive DF images in which we moved the aperture along the arc to capture electrons from different parts of the arc, representing crystals with different azimuthal orientation. In this way we could visualize, in turn, a larger fraction of the crystals which were capable of scattering from their (002) lattice planes. DF images made with different aperture placements were superimposed, using colors to differentiate the multiple aperture settings. To accommodate drift associated with SAED aperture placement, the images were realigned between placements. If, at a point on a DF image made using a specific position on a diffraction ring, we see no illumination then we can conclude that at that point in the sample either: (a) none of the apatite crystals were aligned so as to scatter electrons into the image from the plane used to create the DF image; or (b) there are no apatite crystals in that region.

A given DF image is geometrically equivalent to the BF image of the same field of view, so that any bright spot in the DF image should be correlated with an electron-dense (dark) object in the BF image, and would represent a crystal or polycrystalline structure. Most of these objects would be mineral lamellae visible in the BF images. To test where apatite crystals were also located projected onto (and possibly included within) gap zones, we used the following strategy. Using the BF image of each field of view, we used Photoshop (version CS6) to outline the positions of well-defined gap zones, approximating the edges of the gap zones as straight lines. These lines

were then transferred onto the corresponding aligned DF images in order to locate illuminated crystals which were projected on gap zones. Note however that there is a 60% probability that this was due to superposition of objects which were in fact located at different Z heights in the section and not physically inside the gap zone. While all the DF images used here were obtained using the (002) arcs, other diffraction rings could produce illuminated spots as well, although their form would be less useful to identify the form and location of the crystals which is the goal of this study. For example, the brightest ring in the SAED pattern merges the reflections (211), (112), (300), (202) and (301) (the "multi-reflection ring"). One DF image was obtained using this ring to test whether distinctive features were outlined by illuminated crystals.

3. Results

3.1 DF images obtained using the (002) arc

In figure 5 we see a comparison between images of the same field of view in BF and in DF with the SAED aperture placed on a single angular portion of the (002) arc. The BF image (Fig 5a) shows, as usual, stacks of MLs, elongated dark features which we have shown to represent edgewise images of polycrystalline structures [2, 16]. MLs also exist with their flat surfaces in other orientations ranging up to those lying flat in the plane of the section but these cannot be identified because of the low electron contrast when the crystals are viewed face on. Their presence can be inferred, however, from cross-sectional views of cortical bone [2, 17], and from tomographic images of longitudinal sections of bone [18].

The DF image of the same field of view (Fig 6a) shows streaks of illuminated particles that are oriented parallel to the trends of MLs in the BF image. These are comparable to images from our previous dark-field study of ion-milled sections of bone [3]. An important aspect of such images which was not previously discussed is shown in Fig's 6a and b, showing details of the box in Fig 5. Arrows in Fig 6a point to four dark, planar structures in the BF image which we infer to be crystals or aggregates of crystals (i.e., MLs) viewed edgewise in the section. When we turn to the DF image (Fig 6b), two of these MLs (marked by solid arrows in Fig 6a) are illuminated, while the two MLs marked by dashed arrows in Fig 6a are not illuminated even though they had the same azimuthal orientation as the other crystals. Although the c-axis of apatite crystals of bone always lies in the plane of the crystals, this view shows that not all crystals oriented normal to

the plane of the section are illuminated in DF. This arises because, for the crystal to be illuminated, its c-axis must also lie close to the plane of the section. However, 3D studies of the distribution of the c-axes in apatite crystals in bone [15] show that the c-axes are actually distributed in a spheroidal zone with an angular width like that seen in the arcuate distribution of 002 reflections in SAED patterns of bone (Fig 2). Therefore, we infer that the c-axes of the MLs detectable in Fig 6a but not illuminated in Fig 6b must be tilted out of the plane of the section although not by more than 30^0. As a result only part of the apatite crystals in a field of view will be illuminated in a DF image.

3.2 Transfer of gap-zone images from BF to DF images

The position of all the well-defined gap zones on the BF image 5a were marked with lines and the lines were transferred to the DF image (Fig 7) to test whether any illuminated crystals project onto gap zones. We distinguish between two types of illuminated features: a) ones which are clearly extensions of illuminated linear features that occur outside the projected area of the gap zone and by inference, represent DF images of MLs lying outside the fibrils but projected onto them in the TEM image; and b) ones which are limited in extent to the width of the projected area of the gap zone, and do not extend into the neighboring overlap zones on either side of the gap zone (e.g. yellow arrow in Fig 7). Crystals of the former type are presumably components of MLs which are situated between the fibrils. Crystals constrained within the boundaries of a gap zone could be images of "free" crystals physically within a gap zone. In Fig 7 we can definitely recognize five crystals (red arrows) which project onto a gap zone and do not appear to be a continuation of a linear ML-like feature outside that gap zone. Each of these features stands alone, and is not associated with any other illuminated features aligned with it in a direction parallel to the gap zone. These may be images of crystals of apatite within the gap zone, confirming the widely accepted view that the gap zones are the locus of crystals of apatite.

Figures 8a and 9a are BF images of two additional fields of view of the same ion-milled section. Each is accompanied by two DF images obtained using two separate spots on the (002) arc. The two spots tend to illuminate crystals in different regions of the field of view, which may represent slightly different azimuthal orientations in the plane of the TEM image. As in Figure 6, we have marked the positions of the gap zones seen in the associated BF image (Figs 7b and 8b). As

before, we have searched for illuminated features which are not continuations of illuminated crystals associated with MLs.

In Fig. 8b we found one illuminated feature that projected into a gap zone and did not have an extension outside it (red arrow); all the remaining illuminated features were continuations of structures that extended into the adjoining regions (overlap zones). In Fig 9b, we found no examples of illuminated features whose projection could not be traced outside the gap zone. The single illuminated feature found in Fig 7b once again demonstrates the possibility that some crystalline apatite occurs inside the gap zones of bone mineral.

In summary, in two of the three fields of view studied we found a few examples of illuminated images of crystals of apatite that might be projections of crystals actually present inside gap zones. Note however that there is a 60% probability of any crystal seen in the X-Y plane being projected onto a gap zone, whether or not the crystal actually resides in that gap zone. Therefore there is a high probability that even the apparently "free" illuminated crystals in our DF images which do not appear to be continuations of ML-associated features, are also in extrafibrillar mineral lamellae and not actually inside fibrils.

3.3 DF image using the multi-reflection ring

The (002) reflections seen in SAED patterns of longitudinal sections of bone invariably occur in the form of two discrete complementary arcs spanning about 30^0. This has commonly been taken to infer that all the apatite crystals in bone are oriented with their c-axes parallel to the fibril axes [15]. If apatite crystals occur inside gap zones of collagen fibrils and are large enough to Bragg-scatter electrons, it would seem that their c-axes must also show the same orientation and they should be detectable by the procedure just described. However it is possible that the intrafibrillar apatite crystals have some other orientation but are not sufficiently numerous to show up as subsidiary peaks on the SAED pattern at the scattering angle for (002). In that case it might be that another Bragg reflection than (002) might capture their orientation. To test this, we prepared a DF image using electrons from the multi-reflection ring ((211), (112), (300), (202) and (301) reflections) (Fig 10). Illuminated spots are seemingly randomly distributed across this image. They are not oriented parallel to the MLs nor is any alignment parallel to the gap zones visible by comparison with the BF image. These represent reflections from the five listed lattice

planes. While approximately 60% of these reflections would of necessity project onto a gap zone, there is no evidence of their concentration along these features. It is also important to note that this study employs non-uniformly thick ion milled samples and mass-thickness contrast is further contributing to the ambiguity of the spatial organization the mineral constituents.

4. Discussion

4.1. Comparison with previous studies

In our previous study of dark field images of bone, using the (002) reflection on longitudinal ion-milled sections of bone [3], we exploited the fact that the DF images could not only show the presence of crystals in the field of view but could also show, through similarities in the form and size of their images, how the crystals might be contained within structures already recognized in corresponding BF images. In this way, we showed that the dark, elongated structures that are oriented parallel to the fibril axes are composed of crystals of apatite of the same thickness as the structures and arrayed along those structures. The present study has confirmed that previous observation. However, we were only able to identify a small number of crystals that projected along gap zones and were not extensions of images of MLs. Images presented in our previous study also did not appear to show any strong concentrations of crystals aligned with gap zones; however no special care was taken in that study to investigate this question.

There have been several previous TEM studies of bone which used dark field methods [19–24] . Only the study by Arsenault [19] provides a close comparison to the present study. In this work, DF images of rat bone were obtained using the (002) arc, and reveals a small number of illuminated points that appear to track the positions of gap zones seen in the BF; however, the sample was prepared using an ultramicrotome and some disruption of MLs could have occurred [25]. Using the multi-reflection ring, very few illuminated crystals are visible, with no consistent pattern either parallel or perpendicular to the fibrils [19].

The studies of mineralized turkey leg tendon (MTLT) provide an interesting contrast to the present work (Fig 10) [24]. This material is only partially mineralized and results in the formation of limited areas of mineralized tendon tissue. BF images show a high degree of mineralization of the gap zone [23]. Comparative BF and DF images of a longitudinal section of MTLT are shown in Fig. 11a,b, the DF images obtained using the (002) arc. In striking contrast

to DF images of bone, both the gap and overlap zones are filled with bright spots, with the highest concentration being in the gap zones whose edges are sharply delimited by a reduction in abundance of bright spots. The illuminated features appear to be single crystals elongated parallel to the fibril axis, but the images in [10] are not well-enough resolved to characterize their form. They are on the order of 6 nm in width, consistent with edgewise views of crystals of bone apatite. Fig 11c shows the image obtained with the multi-reflection ring: unlike the images of bone, we continue to see illuminated strips that track the gap zones. It would appear that a large part of the mineral in MTLT is located in the gap zone. Some mineral also occurs as extrafibrillar plates, seen as well in BF images of MTLT in other papers [26–28]. Without trying to speculate as to its cause, it is clear that the pattern of mineralization in MTLT is significantly different from that in bone. However, the images of an illuminated gap zone such as Fig 10b and c could be taken as a model of what we would have been looking for in our DF images of bovine bone, and the absence of which contributed to our belief that the gap zones in that material contained few if any crystals. MTLT remains heavily studied today using TEM, EELS, and diffraction techniques to investigate biomineralization and its unique ultrastructure (e.g.).

4.2. Justification of the use of the (002) arcs

All the DF images shown here and in our earlier work were obtained using the (002) arcs. It could be argued that the crystals situated in the gap zone might be oriented so that the (002) reflections were hardly present. For example, in SAED images of cross sections of long bone the (002) arc is only faintly present in the form of discrete spots, rather than as a continuous ring (e.g.,Fig 2b in [30]). This is because in a cross section of bone, most of the c-axes of apatite crystals are oriented almost normal to the section plane and therefore would not provide Bragg reflections. But perhaps the c-axes of crystals in the gap zone are located at a steep angle to the collagen fibrils; in that case they not be illuminated in a DF image.

However this would be contradictory to the observation that all the apatite crystals in bone tend to be oriented parallel to the fibril axes as a result of which the (002) reflection form an arc and not a complete circle. This phenomenon of parallelism between the apatite c-axes and the fibrils has also been observed when collagen is mineralized *in vitro*. This is shown, for example, by Nudelman et al., [31, 32] who precipitated plates of apatite 2-5 nm thick inside synthetic collagen fibrils. In the study of mineralized turkey tendon by Arsenault an SAED pattern showed

that the apatite crystals, most of which were in the gap zone, were oriented within 35^0 of the fibril axis (Fig 3 in [24]). This is presumably a result of epitaxial crystallization which is relied upon by many organisms to control the orientation of mineral formed in association with protein (e.g. [33]). We would therefore expect that apatite crystals inside the gap zone of bone would also be oriented this way, and would be illuminated in DF images created using the (002) reflection.

It might also be argued that we have used only a small number of points on the (002) arc to search for the presence of illuminated crystals inside the gap zones. However, we showed earlier (Fig. 4) that changing the position of the DF aperture on the arc leads to illumination of crystals with different azimuthal orientations but which are still oriented approximately parallel to the fibril axes. Use of more DF aperture positions would therefore illuminate a larger number of "free" crystals but these would be as sparse as those reported on above. Likewise DF images using different aperture positions on the (002) arc in earlier papers [3, 19] did not provide evidence of gap zones being defined by concentrations of illuminated spots. It may be significant that in the present study we did observe a total of five "free" crystals in the DF images that could possibly be projections of images of crystals inside gap zones. However, given the fact that there is a 60% probability that any illuminated crystal would project onto a gap zone, whether or not it was physically located inside that structure, it would seem that this small number of images of "free" crystals (i.e., not parts of MLs) was more likely the result of the accidental placement of the crystals in MLs above or below a collagen fibril.

Also, note that we are assuming that a crystal whose image extends across the border of a gap zone and into the adjacent overlap zone is not physically located in the fibril. The reason for this judgement is that, in well-focused BF images of bone, the boundary between gap zone and overlap zone is always sharp (see, e.g., Fig. 5a, 9a). This shows that, whatever is the more electron dense material in the gap zone, it does not physically extend across the gap/overlap zone boundary, contrary to claims by some other workers (e.g., [7]).

4.3. What is in the gap zones?

Previous EELS studies of the gap and overlap zones have shown that Ca and P are present in higher concentration in the gap zones than the overlap zones although Ca and P appeared to be present in both at concentrations well above background noise [9, 11]. In most previous literature (e.g [9]) this material is assumed to be crystalline apatite. Olszta et al. [34] present SAED patterns of isolated fibrils from equine cortical bone. Their Fig 4a shows a fibril on which are superimposed electron-opaque elongated structures which we can recognize as edgewise views of apatite crystals. A SAED of this field of view displays diffraction rings appropriate to apatite. In another figure (4c) however, they show the BF image of a single isolated fibril in which no crystals are visible, but which displays typical electron-dense gap zones. Strikingly, the SAED pattern of this fibril shows no rings or spots which would be indicative of the presence of apatite. Olszta et al state that this figure "[suggests] that the electron dense phase, which is the only thing providing contrast (the sample was not stained), is amorphous CaP.".

Only apatite, and not any other crystalline Ca-PO4 phases (such as OCP, whitlockite, etc.) are present in bone at levels that can be detected by X-ray diffraction [35]. Therefore the failure to identify crystals in this region cannot be due to choice of an inappropriate Bragg reflection with which to construct the dark field images. Therefore it appears that the material inside the gap zone is either crystals of apatite too small to Bragg-scatter electrons, or amorphous Ca phosphate (ACP).

The question of whether the material in the gap zone could be ACP is too complex to be discussed here, but is worthy of further investigation. Such a study would have to include issues such as the well-known observation that ACP is intrinsically unstable. When prepared in the laboratory it rapidly (within a few hours) crystallizes to a Ca phosphate mineral, usually apatite. Nuclear magnetic resonance (NMR) studies of bone have suggested that significant amounts of ACP are present in bone, although in close spatial association with crystalline apatite [36].

5. Conclusion

In this work we employed correlative BF and DF TEM of ion milled bovine bone to investigate the organization of the mineral component of bone ultrastructure, specifically the location of the mineral with respect to the gap zone. Superposition of the DF images collected using SAED

placement on the (002) apatite reflection demonstrated that most apatite crystals were not confined to the gap zones. Meanwhile, a number of "free" crystals did not extend into the overlap zone, demonstrating potential to be within the gap zone. However, we suggest this may be an attributed to projections of gap zones within the sample. In comparison, the results presented in this work suggest a likelihood of mineral residing outside of the gap zone and we speculate that the mineral in the gap zone may be ACP.

6. Acknowledgements

DMB was supported partially by an Ontario Graduate Scholarship and an NSERC CGS-M. LL prepared samples and helped perform TEM. TEM was performed at the Canadian Centre of Electron Microscopy (CCEM), a facility supported by NSERC and other governmental sources. We thank Carmen Andrei for assistance with TEM operation. Our thanks extends to Martin Knyf of the School of Geography and Earth Science at McMaster University for his assistance with sample preparation. This research was funded by grants from the Natural Sciences and Engineering Research Council of Canada held by both KG and HPS.

7. References cited

1. McNally E, Schwarcz H, Botton G, Arsenault A (2012) A model for the ultrastructure of bone based on electron microscopy of ion-milled sections. PLoS One 7: . doi: 10.1371/journal.pone.0029258

2. Grandfield K, Vuong V, Schwarcz HP (2018) Ultrastructure of Bone: Hierarchical Features from Nanometer to Micrometer Scale Revealed in Focused Ion Beam Sections in the TEM. Calcif Tissue Int 0:0 . doi: 10.1007/s00223-018-0454-9

3. Schwarcz HP, McNally EA, Botton GA (2014) Dark-field transmission electron microscopy of cortical bone reveals details of extrafibrillar crystals. J Struct Biol 188:240–248 . doi: 10.1016/j.jsb.2014.10.005

4. Weiner S, Price PA (1986) Disaggregation of bone into crystals. Calcif Tissue Int 39:365–375 . doi: 10.1007/BF02555173

5. Schwarcz HP (2015) The ultrastructure of bone as revealed in electron microscopy of

ion-milled sections. Semin Cell Dev Biol 46: 44–50 . doi: 10.1016/j.semcdb.2015.06.008

6. Weiner S, Traub W (1992) Bone structure: from angstroms to microns. FASEB J 6:879–885 . doi: 10.1096/fasebj.6.3.1740237

7. Landis (1993) Mineral and Organic Matrix Interaction in Normally Calcifying Tendon Visualized in Three Dimensions by High-Voltage Electron Microscopic, Landis.pdf. J Struct Biol 110:39–54

8. Jäger I, Fratzl P (2000) Mineralized collagen fibrils: A mechanical model with a staggered arrangement of mineral particles. Biophys J. 79(4): 1737-1746 doi: 10.1016/S0006-3495(00)76426-5

9. Alexander B, Daulton TL, Genin GM, et al (2012) The nanometre-scale physiology of bone: steric modelling and scanning transmission electron microscopy of collagen-mineral structure. J R Soc Interface 9:1774–1786 . doi: 10.1098/rsif.2011.0880

10. McNally EA, Schwarcz HP, Botton GA, Arsenault AL (2012) A model for the ultrastructure of bone based on electron microscopy of ion-milled sections. PLoS One 7:1–12 . doi: 10.1371/journal.pone.0029258

11. Jantou-Morris V, Horton MA, McComb DW (2010) The nano-morphological relationships between apatite crystals and collagen fibrils in ivory dentine. Biomaterials 31:5275–5286 . doi: 10.1016/j.biomaterials.2010.03.025

12. Williams D, Carter B (1996) Transmission electron microscopy. Plenum, New York

13. Lee BEJ, Luo L, Grandfield K, Andrei C and Schwarcz HP (2019) Identification of collagen fibrils in cross sections of bone by electron energy loss spectroscopy (EELS). Micron 124: 102706. doi: 10.1016/j.micron.2019.102706

14. Tong W, Glimcher MJ, Katz JL, et al (2003) Size and shape of mineralites in young bovine bone measured by atomic force microscopy. Calcified Tissue International. 5: 592–598

15. Wenk HR, Heidelbach F (1999) Crystal alignment of carbonated apatite in bone and

calcified tendon: Results from quantitative texture analysis. Bone 24:361–369 . doi: 10.1016/S8756-3282(98)00192-6

16. Schwarcz HP, McNally EA, Botton GA (2014) Dark-field transmission electron microscopy of cortical bone reveals details of extrafibrillar crystals. J Struct Biol 188: 240-248 . doi: 10.1016/j.jsb.2014.10.005

17. Schwarcz HP (2015) The ultrastructure of bone as revealed in electron microscopy of ion-milled sections. Semin Cell Dev Biol 46:44–50 . doi: 10.1016/j.semcdb.2015.06.008

18. McNally E, Nan F, Botton GA, Schwarcz HP (2013) Scanning transmission electron microscopic tomography of cortical bone using Z-contrast imaging. Micron 49:46-53 . doi: 10.1016/j.micron.2013.03.002

19. Arsenault AL (1989) A comparative electron microscopic study of apatite crystals in collagen fibrils of rat bone, dentin and calcified turkey leg tendons. Bone Miner. 6(2): 165-177 doi: 10.1016/0169-6009(89)90048-2

20. Arsenault AL, Grynpas MD (1988) Crystals in calcified epiphyseal cartilage and cortical bone of the rat. Calcif Tissue Int. 43(4) 219-225 doi: 10.1007/BF02555138

21. Arsenault AL, Hunziker EB (1988) Electron microscopic analysis of mineral deposits in the calcifying epiphyseal growth plate. Calcif Tissue Int. 42(2) 119-126 doi: 10.1007/BF02556344

22. Jackson SA, Cartwright AG, Lewis D (1978) The morphology of bone mineral crystals. Calcif Tissue Res. 25(1) 217-222 doi: 10.1007/BF02010772

23. Tracy BM, Doremus RH (1984) Direct electron microscopy studies of the bone—hydroxylapatite interface. J Biomed Mater Res 18(7) 719-726. doi: 10.1002/jbm.820180702

24. Arsenault AL (1988) Crystal-collagen relationships in calcified turkey leg tendons visualized by selected-area dark field electron microscopy. Calcif Tissue Int. 43(4) 202-212 doi: 10.1007/BF02555136

25. Jantou V, Turmaine M, West GD, et al (2009) Focused ion beam milling and ultramicrotomy of mineralised ivory dentine for analytical transmission electron microscopy. Micron 40:495–501 . doi: 10.1016/j.micron.2008.12.002

26. Traub W, Arad T, Weiner S (2006) Three-dimensional ordered distribution of crystals in turkey tendon collagen fibers. Proc Natl Acad Sci. 86(24) 9822-9826 doi: 10.1073/pnas.86.24.9822

27. Weiner S, Traub W (1986) Organization of hydroxyapatite crystals within collagen fibrils. FEBS Lett. 206(2) 262-266 doi: 10.1016/0014-5793(86)80993-0

28. Traub W, Arad T, Weiner S (1992) Growth of mineral crystals in Turkey tendon collagen fibers. Connect Tissue Res. d 28(1-2) 99-111 oi: 10.3109/03008209209014230

29. Kłosowski MM, Carzaniga R, Shefelbine SJ, et al (2018) Nanoanalytical electron microscopy of events predisposing to mineralisation of Turkey tendon. Sci Rep. 8, Article number: 3024 doi: 10.1038/s41598-018-20072-2

30. Tertuliano OA, Greer JR (2016) The nanocomposite nature of bone drives its strength and damage resistance. Nat Mater. 15(11) 1195-1202 doi: 10.1038/nmat4719

31. Nudelman F, Pieterse K, George A, et al (2010) The role of collagen in bone apatite formation in the presence of hydroxyapatite nucleation inhibitors. Nat Mater. doi: 10.1038/nmat2875

32. Nudelman F, Lausch AJ, Sommerdijk NAJM, Sone ED (2013) In vitro models of collagen biomineralization. J Struct Biol. 183(2) 258-269 doi: 10.1016/j.jsb.2013.04.003

33. Nudelman F (2015) Nacre biomineralisation: A review on the mechanisms of crystal nucleation. Semin. Cell Dev. Biol 46:2-10. doi: 10.1016/j.semcdb.2015.07.004

34. Olszta MJ, Cheng X, Jee SS, et al (2007) Bone structure and formation: A new perspective. Mater. Sci. Eng. R Reports 58, Issues 3–5. oi.org/10.1016/j.mser.2007.05.001

35. Elliott JC (2002) Calcium Phosphate Biominerals. Rev Mineral Geochemistry 48:427–453. doi: 10.2138/rmg.2002.48.11

36. Von Euw S, Chan-Chang T-H-C, Paquis C, et al (2018) Organization of Bone Mineral: The Role of Mineral–Water Interactions. Geosciences. 8, 466 .doi: 10.3390/geosciences8120466

7. Figures

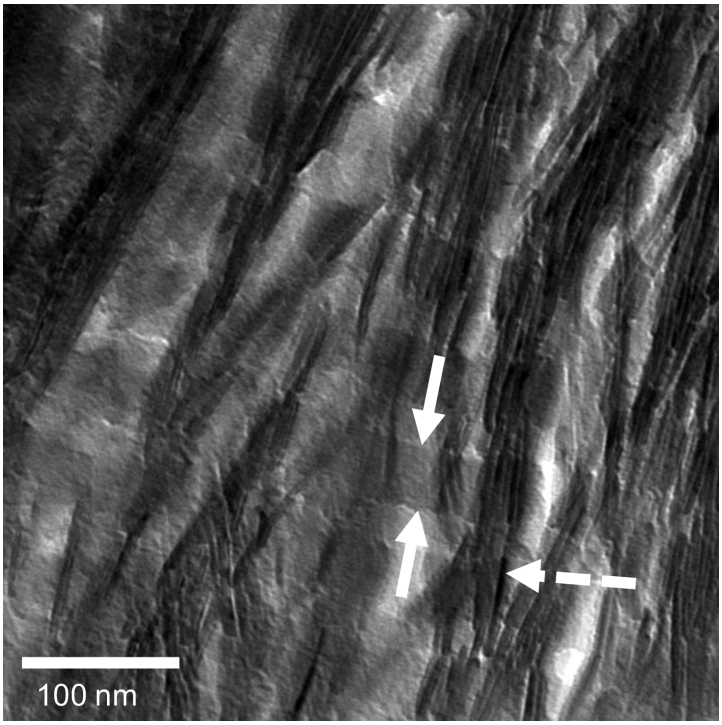

1. Bright field TEM image of section of human femoral bone cut parallel to the femoral axis. Solid arrows: gap zone, showing higher electron contrast due to presence of higher Z number material; Dashed arrow: mineral lamellae oriented parallel to long axis of collagen fibrils. Note that gap/overlap zones extend continuously across field of view even though individual fibrils are only 50 nm in diameter. This is because the fibrils are in registry in three dimensions (see text). Scale = 100 nm. Adapted from [16] with permission from Elsevier.

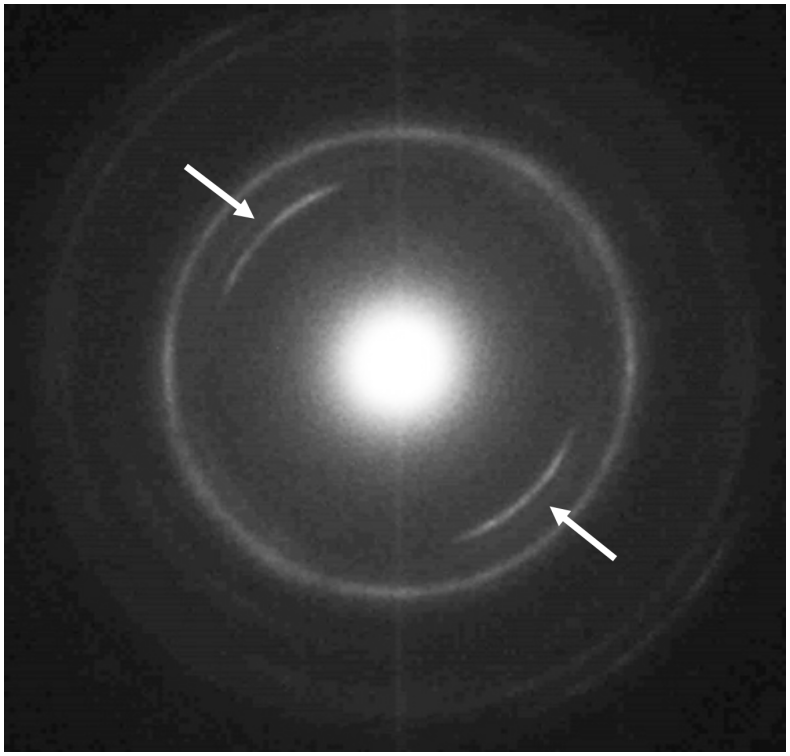

2. Selected-area electron diffraction pattern of bovine cortical bone. Dashed arrows: (002) reflection of apatite crystal lattice in the form of two symmetrical arcs of about 30^0, corresponding to preferred orientation of c-axes of apatite crystals in bone parallel to the collagen fibrils. Dashed arrow: strongest ring comprised of reflections from (211), (112), (300), (202) and (301) planes of apatite.

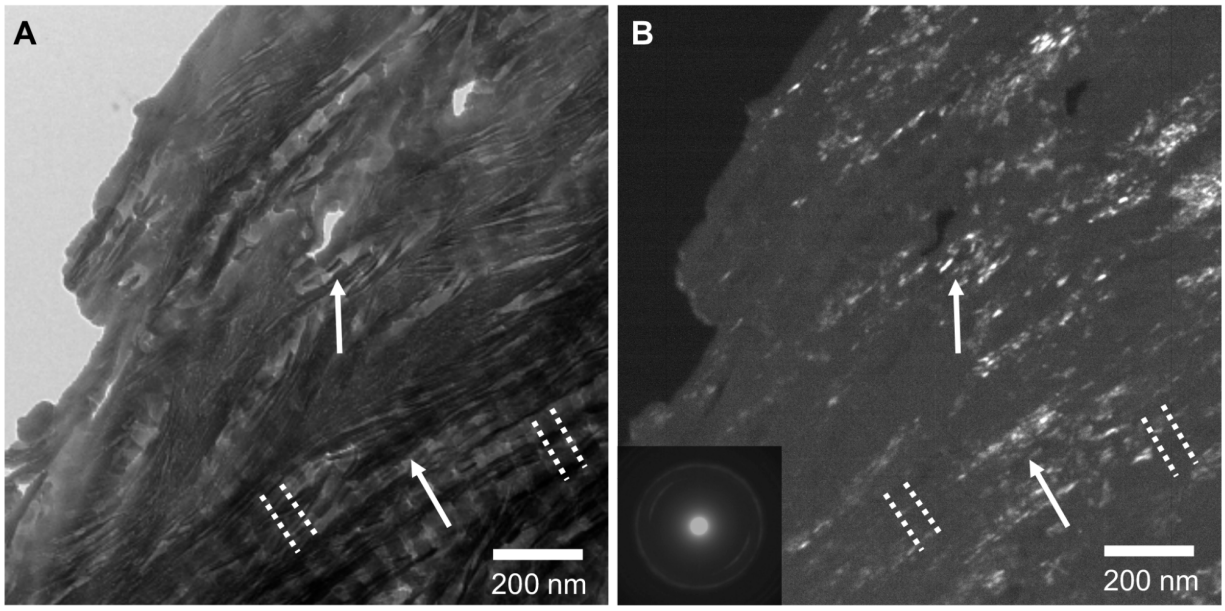

3. Schematic view of part of an ion-milled section of bone cut parallel to the long axis of a long bone. The BF TEM image would be of the X-Y plane. In the X-Z plane we see cross sections of collagen fibrils (red diamond) which have been largely eroded by the ion beam [13]. Note that any given line drawn normal to the X-Y plane (i.e., parallel to Z-axis) would pass through one or more collagen fibrils. Red arrow: end-on view of single mineral lamella oriented parallel to Y-Z plane. This lamella would be visible as a dark feature in the BF TEM image (X-Y plane). Yellow arrow: end on view of mineral lamella oriented parallel to X-Y plane and hence not detectible on the BF TEM image.

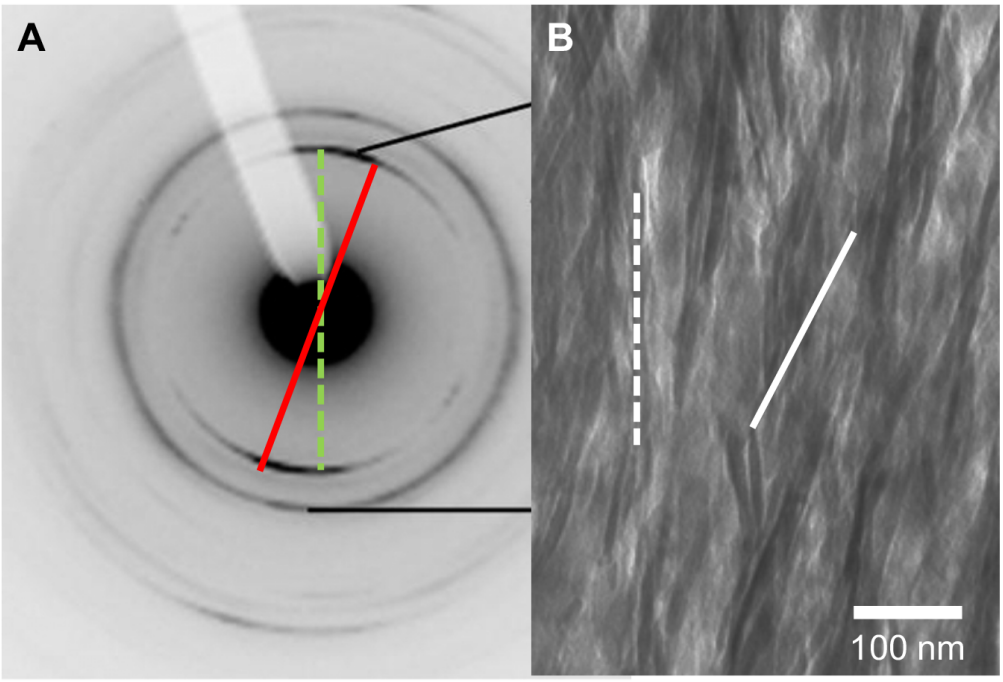

4. TEM image of ion milled section of bovine bone with accompanying SAED image , showing the effect of moving the SAED aperture to two distinct symmetric pairs of points on the (002) arc; the azimuth of the ML whose crystals are illuminated would rotate by an angle equal to the change in angle of the line connecting the two aperture points. The majority of MLs are aligned parallel to the green line (as shown by the concentration of electron density on the arc), whereas fewer MLs are aligned parallel to the red line (whose aperture points lie near the end of the (002) arc). Scale = 50 nm

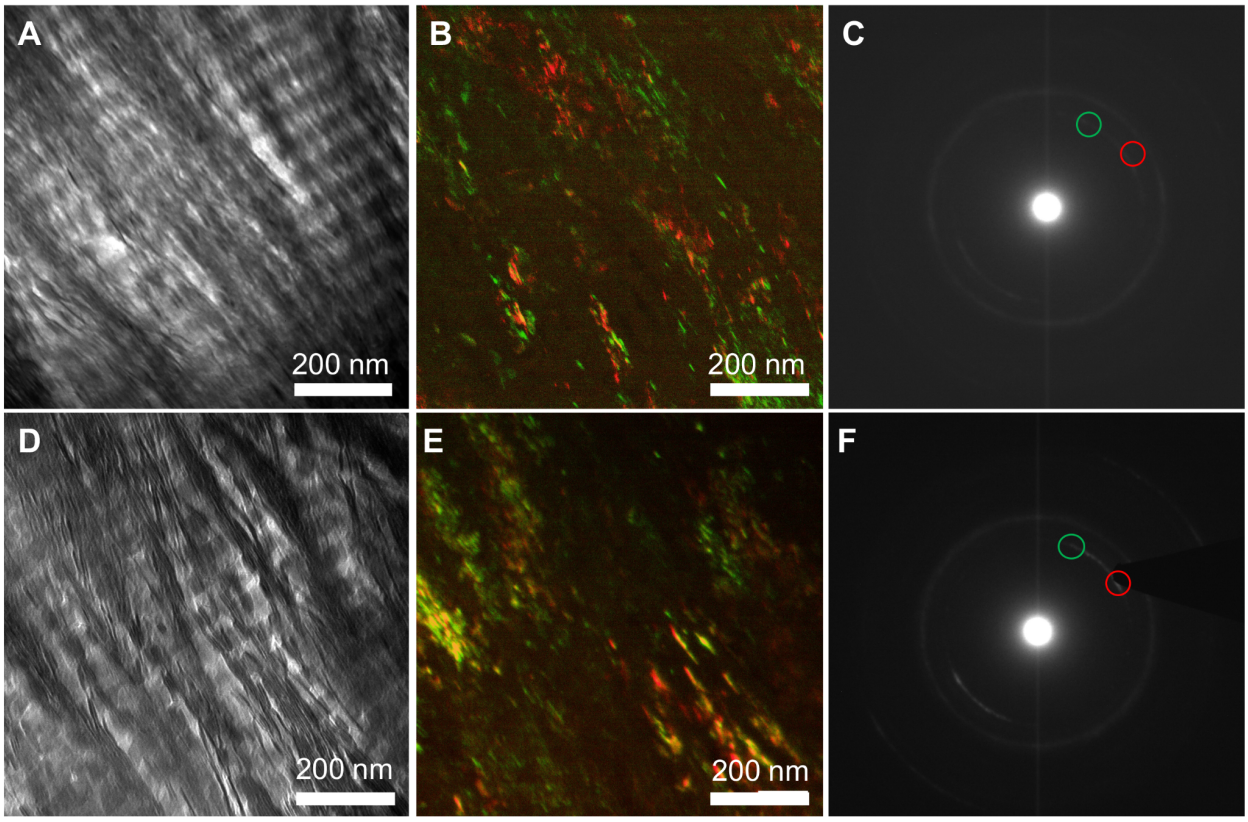

5. TEM images of ion milled longitudinal section of cortical bone from bovine femur: a) Bright-field image. Dashed arrow: stack of mineral lamellae; solid arrow: gap zone surrounded by two less electron-dense (lighter) overlap zones. Gap zone orientation appears to extend continuously for about 1 μm. b) Dark field image of same field of view; SAED aperture place on one of the 002 arcs (not shown): solid arrow: single illuminated feature representing edgewise view of single crystal of apatite 5 nm thick and about 40 nm long; dashed arrows: multiple illuminated apatite crystals aligned parallel to mineral lamellae; note that most of the illuminated crystals have this orientation. Dashed lines on both images outline some of the gap zones within collagen fibrils; in (a) note that gap zones extend over much longer distances than the width of single fibrils showing that they must be the projected image of gap zones in multiple fibrils which overlap in three dimensions. Also note that they are sharply demarcated against the adjacent overlap zones (see Fig 1) . Box = area of Fig 6. Scale = 200 nm

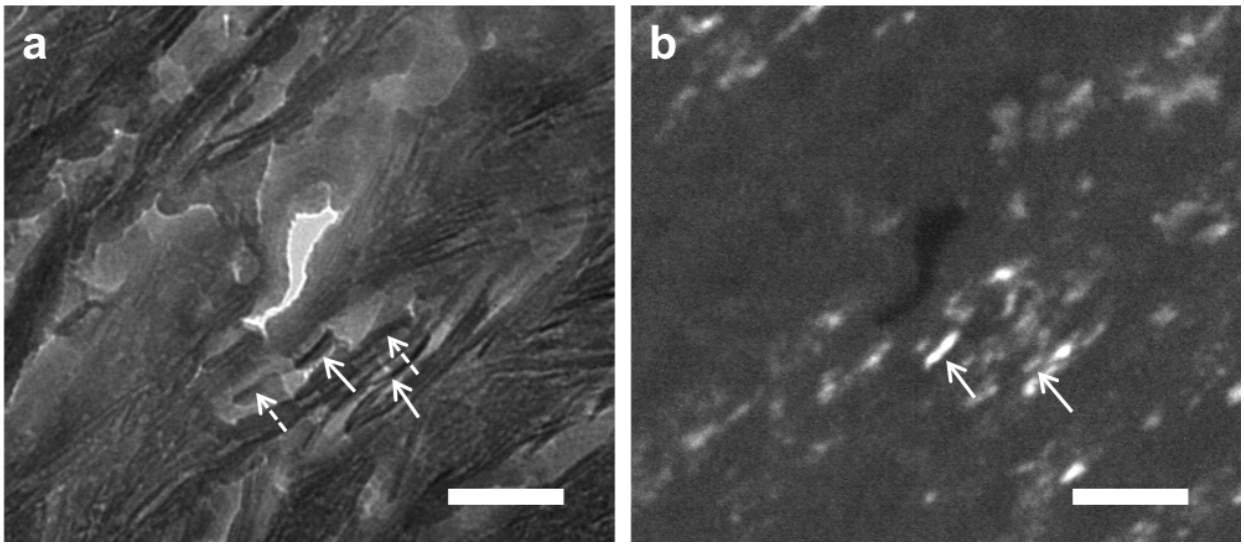

6. Digitally magnified detail of area of Fig. 5: a) Bright field image: solid arrows: crystals that are illuminated in DF; dashed arrows: crystals that are not illuminated in DF; scale = 100 nm; b) DF image of same field of view; only two of the dark features marked in (a) are illuminated, presumably because c-axes of the other two, although lying in the plane of these flattened crystals, are tilted out of the plane of the section.

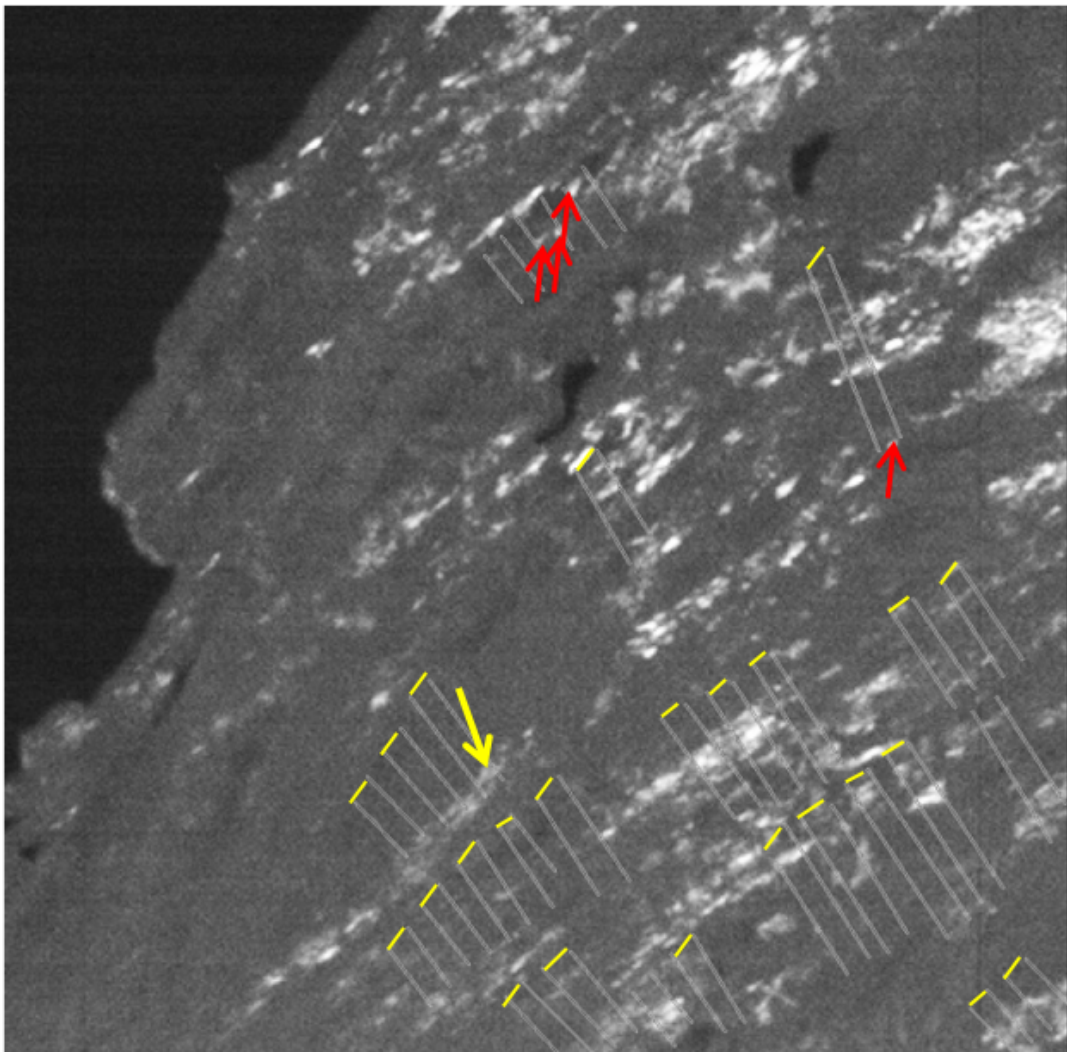

7. DF image from Fig 5, with gap zones outlined (dashed lines; yellow bars show interior of each gap zone). The red arrows indicate the five illuminated particles whose images project entirely within a gap zone. All other illuminated particles projected into gap zones are extensions of features also found in the adjacent overlap zone.

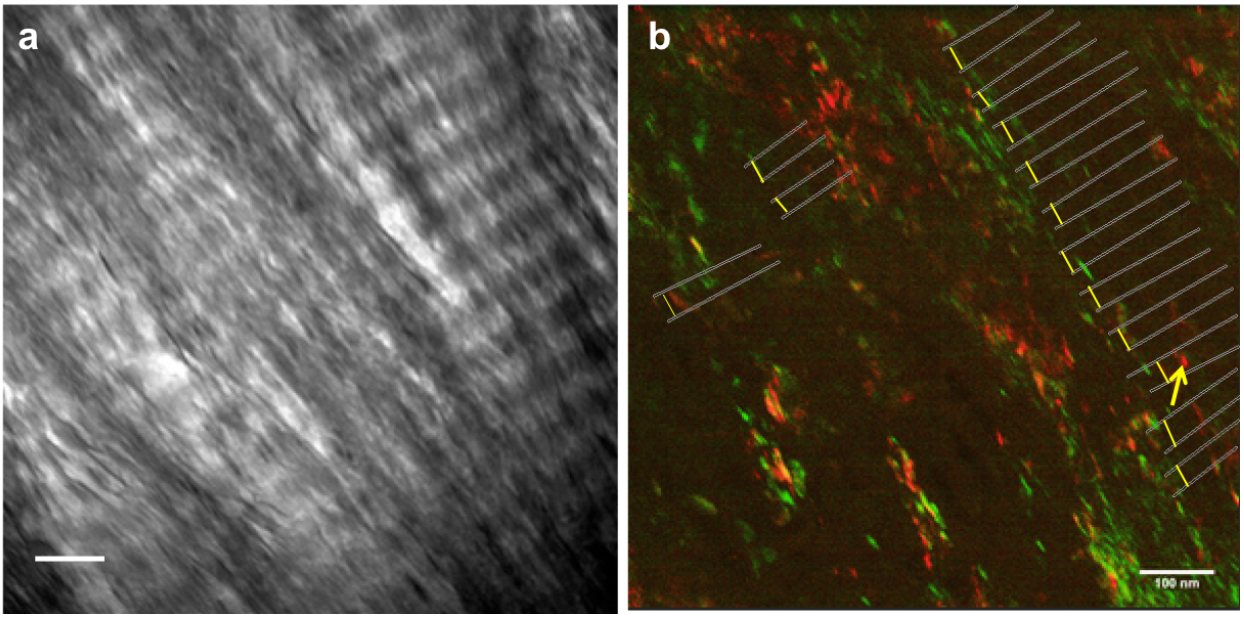

8. TEM images of a second field of view of the ion milled section of bovine cortical bone. a) BF image; scale = 100 nm ; b) two DF images obtain from two points of the (002) arc, one image is projected in red, the other in green. Dashed lines show the outlines of gap zones transferred from the BF image; yellow bars show interior of each gap zone. Only one illuminated particle (yellow arrow) appears to be projected onto the interior of a gap; other illuminated particles projected onto the positions of gap zones are extensions of features also found projected onto the adjacent overlap zones.

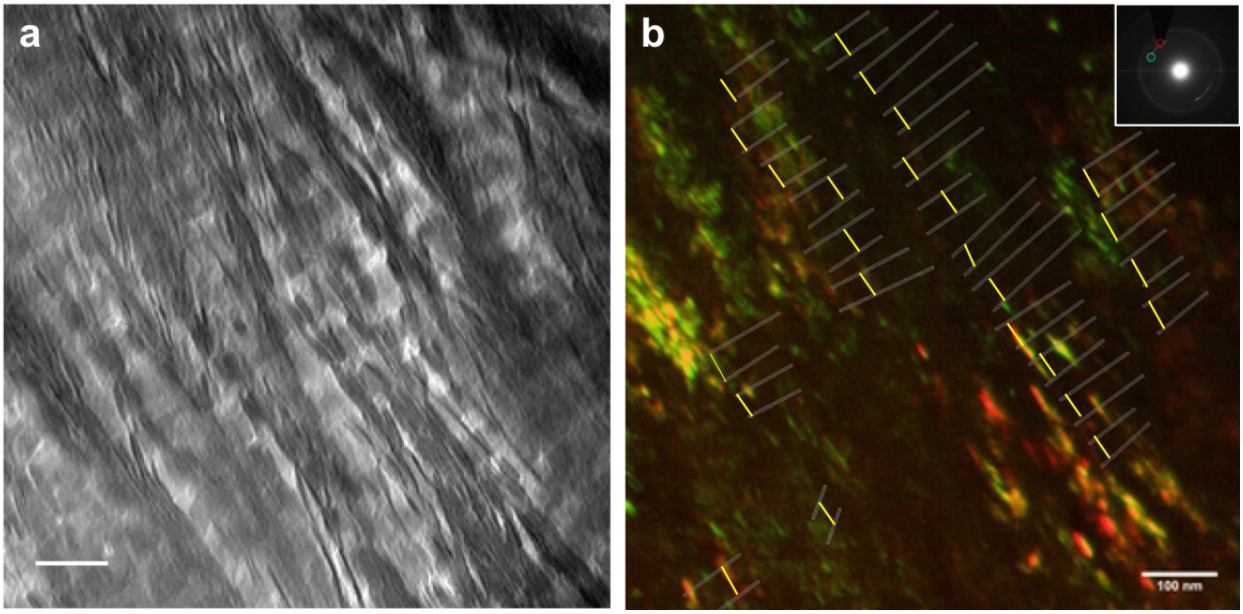

9. TEM images of a third field of view of the ion milled section of bovine cortical bone. a) BF image; scale = 100 nm ; b) two DF images obtain from two points of the (002) arc, one image is projected in red, the other in green. Dashed lines show the outlines of gap zones transferred from the BF image; yellow bars show interior of each gap zone. All illuminated particles projected onto the positions of gap zones in this image are extensions of features also found projected onto the adjacent overlap zones. Inset: shows positions of apertures on the (002) arc; similar positions were used for Fig

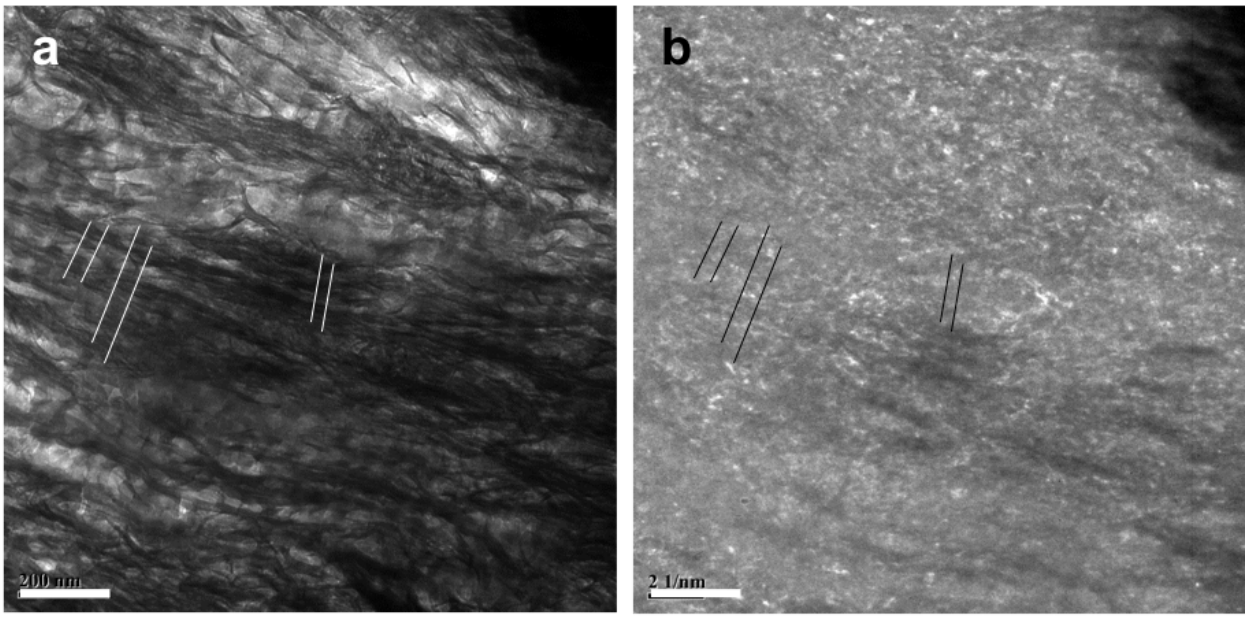

10. TEM images of ion-milled section of bovine femur. a) BF image; scale = 200 nm; b: DF image using multi-reflection ring, where lines represent examples of gap zones.

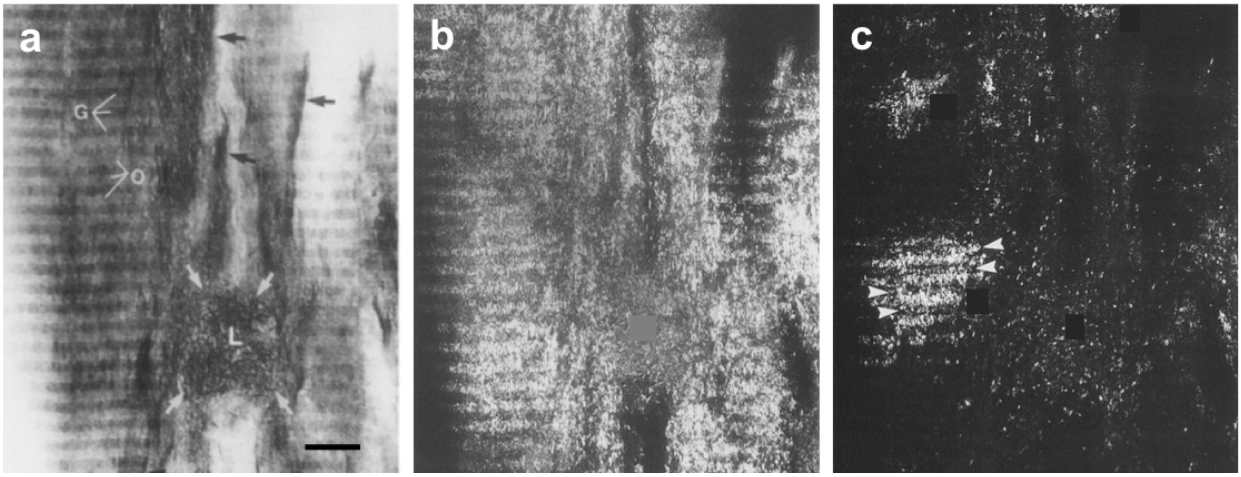

11. TEM images of ion-milled section of mineralized turkey leg tendon (MTLT); a) BF image; scale = 200 nm; b: DF image using the (002) ring; note large numbers of illuminated features aligned with the gap zone, although poorly resolved, it appears that the illuminated objects are elongated parallel to the fibril axis ; c) DF image using the multi-reflection ring. Image adapted from [24] with kind permission from Springer Nature.